AIP | Journal of Applied Physics

Electro-degradation and resistive switching of Fe-doped SrTiO3 single crystal

M. Wojtyniak, K. Szot, R. Wrzalik, C. Rodenbücher, G. Roth et al.

Citation: J. Appl. Phys. **113**, 083713 (2013); doi: 10.1063/1.4793632
View online: http://dx.doi.org/10.1063/1.4793632
View Table of Contents: http://jap.aip.org/resource/1/JAPIAU/v113/i8
Published by the American Institute of Physics.

JOURNAL OF APPLIED PHYSICS **113**, 083713 (2013)

Electro-degradation and resistive switching of Fe-doped $SrTiO_3$ single crystal

M. Wojtyniak,[1,2,a)] K. Szot,[1,2] R. Wrzalik,[2] C. Rodenbücher,[1] G. Roth,[3] and R. Waser[1,4,5]
[1]*Peter Grünberg Institut, Forschungszentrum Jülich, 52425 Jülich, Germany*
[2]*Institute of Physics, University of Silesia, 40-007 Katowice, Poland*
[3]*Institute of Crystallography, RWTH Aachen University, 52056 Aachen, Germany*
[4]*Institut für Werkstoffe der Elektrotechnik, RWTH Aachen University, 52056 Aachen, Germany*
[5]*JARA Fundamentals for Future Information Technology, Jülich, Germany*

(Received 14 January 2013; accepted 12 February 2013; published online 27 February 2013)

In this work, the results of the electrocoloration of strontium titanate single crystals with different iron concentrations are presented. The samples of $SrTiO_3(100)$ doped with 0.06 at. % and 0.13 at. % of iron were electroreduced at low pressure (10^{-8} mbar) and elevated temperature (250 °C) using a DC voltage of 200 V. This led to the migration of oxygen vacancies and subsequent electrocoloration of the samples, which was confirmed by optical analysis and electrical measurements. Evolution of the color front was compared with finite element calculations of electric potential indicating good agreement. Both macroscopic and nanoscopic measurements showed insulator-metal transition at several hundreds of seconds (0.06%Fe) and resistive switching behavior. We found that the resistive switching is clearly modified by the oxygen partial pressure of the ambient atmosphere. Moreover, after electroreduction, in the region between the electrodes, stripes can be found following simple crystallographic directions connected with the extended defects and easy diffusion paths also observed in the single crystals of undoped strontium titanate. Furthermore, migration of negatively charged oxygen ions towards the anode led to the formation of oxygen bubbles trapped between the surface of the crystal and the electrode. Using atomic force microscopy, we were able to measure the geometry of a bubble and calculate the oxygen pressure necessary for the formation of such bubbles and the total amount of oxygen ions trapped within. © *2013 American Institute of Physics*. [http://dx.doi.org/10.1063/1.4793632]

I. INTRODUCTION

Strontium titanate ($SrTiO_3$—STO) is an insulator with a 3.2 eV band gap, and thanks to its simple cubic structure in a wide temperature range,[1] it is considered to be a model perovskite material. The range of applications of STO is very wide, while one of the latest implementations is the substrate for the high-Tc superconductors[2] and the high-k dielectric for CMOS.[3] Recently, STO has received a great deal of scientific attention due to the resistive switching (RS) phenomena[4] and is a good candidate for building a new type of memory—the resistive random access memory (RRAM).[5] It was discovered that the metal-insulator (MI) transition is necessary for RS behavior and that the origin of MI in perovskites is due to the difference in the oxygen vacancy concentration along the network of extended defects.[6] The extended defect can act as an easy diffusion path enhancing ionic conductivity by at least several orders of magnitude, therefore, even moderate thermal treatment under reducing conditions can introduce sufficient oxygen vacancies for the MI transition.[7,8] The other possibility of introducing MI transition is the electric field. In fact, it has been known for over 50 yr that that the dc-voltage stress increases the conductivity of STO single crystals.[9] This is termed electroreduction and is correlated with electrocoloration phenomena. It is observed in many perovskites, and has been investigated in STO by several authors.[6,10] In particular, the results obtained by Waser *et al.*[11] on Al-doped, Ni-doped, and Fe-doped STO single crystals led to some interesting conclusions:

1. In the case of Fe-doped STO, the conductivity increase during the electrodegradation process depends strongly on the iron concentration and was found to be much higher for lower Fe concentrations.
2. Electromigration of oxygen vacancies and the difference in their concentration in the crystal is the basis for the electrocoloration phenomena.
3. The oxygen partial pressure of the ambient atmosphere has no influence on the electrocoloration (electrodegradation) process.

Consequently, the quantitative model for resistance degradation was established on the basis of the point defect chemistry and transport equations.[12] This model proved to be very reliable in several cases such as the calculation of temperature-dependent ambipolar diffusion coefficients[13] or the conductivity profiles after dc stress in iron-doped STO. In similar ternary oxides, the electrocoloration process was also connected with the melting of oxygen vacancy ordering and the associated redistribution of carriers.[14] Equally, the self-order[15] and clustering[16] of oxygen vacancies was also observed in STO.

In general, we found good agreement with the previously reported data, although our results on RS behavior after electrocoloration showed that in fact the STO crystal is an open system and there is a significant exchange of oxygen with the

a)mwojtyniak@us.edu.pl.

surrounding atmosphere. Moreover, due to the inhomogeneous electrical behavior related to extended defects in STO especially on the nanoscale, we believe that it is difficult to successfully describe the properties of investigated material using defect chemistry only. Additionally, in all of the previous electrocoloration experiments, the electrodes were either sputtered or attached to the sides of the investigated samples. Those are not very favorable conditions, since it was shown that the density of dislocations depends on the distance from the surface and is higher in the actual surface compared to the bulk.[17] In the results, the defect concentration close to the surface can be several orders of magnitude higher than in the bulk. Therefore, in our work, we introduced a completely different electrode geometry in order to exclude the edges and sides of the crystal, as can be seen in Fig. 1. Moreover, we used additional electrodes between the anode and cathode to measure the electric potential of each of the electrodes. This gave us the opportunity to calculate the potential drop not only for the whole sample ($\phi_1 - \phi_4$) but also for the anode region ($\phi_1 - \phi_2$), cathode region ($\phi_3 - \phi_4$), and the center (interior) region far from the electrodes ($\phi_2 - \phi_3$). Thus, at any point of the experiment, we were able to characterize the electrical behavior such as $R(T)$ curves or RS, for the anode, cathode, and the interior of the crystals, which is a clear advantage in contrast to standard measurement methods found in many publications. Last but not least, a careful investigation was made of the oxygen bubble formation under the anode electrode, specially considering the geometry of the bubble, the oxygen pressure necessary to form it and calculation of the number of oxygen ions trapped inside visible bubbles.

II. EXPERIMENTAL

The Verneuil-grown single crystals of $SrTiO_3$ doped with 0.06 at. %Fe and 0.13 at. %Fe were cut into $10 \times 10 \times 0.5\,mm^3$ samples and epi-polished from both sides ((100) orientation—CrysTec, Berlin). Platinum electrodes with diameters of 1.0 (anode and cathode) and 0.3 mm (inner electrodes) were formed on top of the crystals. In the case of 0.06%Fe-doped sample, the 20 nm thick Pt electrodes were sputtered and in the case of 0.13%Fe-doped sample the electrodes were attached using high-purity Pt paste. Electrical measurements were preformed with two Keithley 6524 electrometers and a programmable current source Keithley 224, and the temperature was controlled by a Lake Shore 340 temperature controller. The electroreduction procedure was performed at a temperature of ~250 °C under a low pressure of 10^{-8} mbar. The positive dc voltage was applied to one of the anodes with current compliance set to 10 mA (100 mA at further stages). During electroreduction, the potential drop was measured for all electrodes at all times. Local conductivity atomic force microscopy (LC-AFM) measurements were performed using the Omicron STM/AFM VT-50/500 UHV system, equipped with Pt-coated conducting tips.

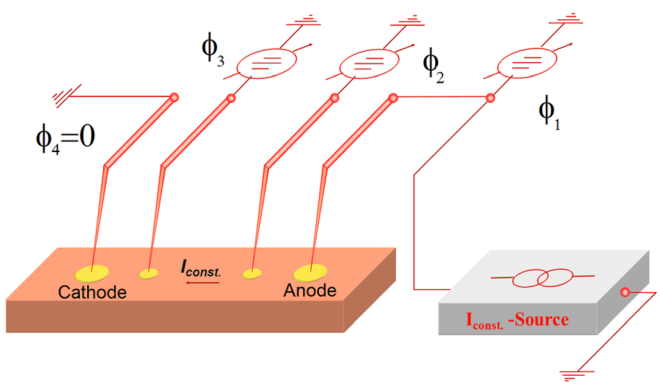

FIG. 1. The sample and electrode geometry along with the experimental setup.

III. RESULTS AND DISCUSSION

Qualitatively, results for both 0.06%Fe and 0.13%Fe doped samples were very similar, although the sample with lower iron concentration was formed significantly faster the color front emerged in a few minutes compared to several days for the sample with higher iron content. Moreover, the sputtered electrodes had much better geometry compared to those attached by paste, therefore, most of the results presented here are for the sample with lower iron content ($SrTiO_3 + 0.06\%Fe$). The color of the as-received crystal was slightly brownish due to the Fe doping. The experiment was started by first heating the sample to 250 °C and then applying the maximum available voltage of 200 V with the current compliance set to 10 mA. At the same time, measurement of the electrical behavior versus time was started. The first 1000 s (approximately 16 min) of electrical behavior can be seen in Fig. 2. It is worth mentioning that the initial resistivity of the sample was roughly equal to 10 MΩ (taken from the first measured value after 5 ms of the experiment) and decreased quickly with time. The resistivity decrease can be seen from the behavior of the total current flowing through the sample (inset of Fig. 2), which increased by roughly 3 orders of magnitude during the first 200 s to the value limited by the current compliance. The qualitative explanation of the electrocoloration process includes the fact that under our experimental conditions (temperature close to 250 °C) only the oxygen vacancies are considered to be mobile and the main point defects in the STO lattice are the Schottky defects.[18] Therefore, the electric field causes the

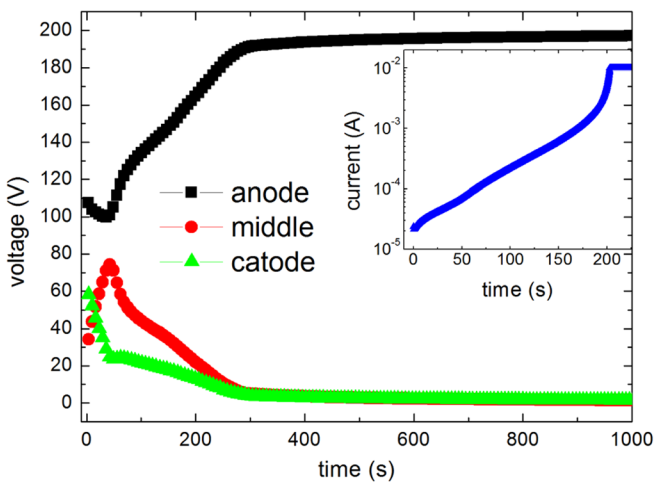

FIG. 2. Electric behavior during electroformation recorded separately for anode, cathode, and middle of the crystal.

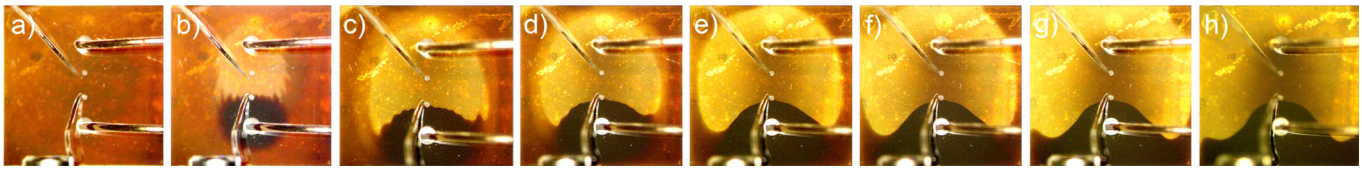

FIG. 3. Optical microscope images of electrocoloration process versus time: (a) 0, (b) 240, (c) 360, (d) 420, (e) 520, (f) 630, (g) 800, and (h) 960 s. Experiment conditions: temperature ~250 °C, pressure 10^{-8} mbar, voltage 200 V, current compliance 10 mA. The bottom electrode is the anode, while the top is the cathode.

movement of charged particles in such a way that the positively charged oxygen vacancies $[V_O^{\cdot\cdot}]$ drift to the negatively charged cathode.[10] The existence of a path consisting of oxygen vacancies after the electrical stress (known as electroformation) was also shown in chromium-doped STO by X-ray absorption near-edge spectroscopy (XANES) experiments.[19] Simultaneously, a voltage drop was observed across the different parts of the crystal and directly correlated with the oxygen vacancy concentration in the crystal in the following manner: increase (accumulation) of oxygen vacancy concentration at the cathode decreases its resistivity, while the opposite process is observed at the anode (Fig. 2). At the same time, optical characterization showed that the two differently colored regions started to grow and moved towards each other until they touched. Next, the two regions grew covering the entire sample volume—Figs. 3(b)–3(h). The details of the dark front movement along with the corresponding voltage drop can be found in Table I. It was shown that the observed colors are characteristic of the reduced and oxidized forms of the iron in a Fe-doped STO single crystal.[10,20] The dark color around the anode originates from the presence of Fe^{4+}, while the light yellow color around the cathode originates from the iron at lower oxidation states Fe^{3+}.[21] More recent examinations by electron paramagnetic resonance, Raman scattering, and X-ray absorption of a very similar system—electroreduced 0.2 wt. % Fe-doped STO single crystal revealed more detailed characteristics, namely, the presence of cubic Fe^{3+} centers with part of axial $Fe^{3+} - [V_O^{\cdot\cdot}]$ in the cathodic region and predominance of Fe^{4+} in the anodic region.[22] The general shape of the color boundary (front) emerging from the electrodes is consistent with the finite element calculations of the in-plane and out-of-plane electric field potential presented in Fig. 4. The calculations assumed homogeneous conductivity of the material. In our case, it can be seen that in the first several hundred seconds of electrocoloration the color front is jagged with characteristic fingers reaching in between the electrodes—Figs. 3(b)–3(d). The observed inhomogeneity is the result of the existence of easy diffusion paths, which enhance the ionic transport. An additional example of enhanced ionic conductivity can be found in Fig. 3(h), where a small disturbance close to the very edge of the crystal can be seen (left side). The bright color there advances further down than in any other part of the crystal at this time. We can easily correlate this with the fact that the surface (or in this case edge) of the crystal has a higher density of defects than the bulk,[17] which will increase the migration speed of the oxygen ions.

With longer experimental times (up to 100 h), the reduced region expands into the oxidized region as seen in Fig. 5. This could be explained by the fact that the ionic current is not completely blocked by the anode and by the crystal surface, and a substantial amount of oxygen is released. Since the oxygen was released only in the region with a high positive electric field (anode), the formation of characteristic bubbles can be observed—Figs. 6(b) and 6(c)—which are formed by the oxygen trapped under the electrode and deforming the electrode material. Other examples of oxygen bubbles formed under similar conditions can be found in various references.[4,23] Detailed characterization of the bubble geometry by the AFM (not presented) gave us the opportunity to approximately calculate the pressure necessary for the formation of such bubbles and to estimate the total amount of oxygen ions trapped inside. For the calculations, we adopted the analytical solution for the bending of a uniformly loaded plate with a radius of a, clamped at the edges[24] as shown in the following equation:

$$h = \frac{P_0 a^4}{64D}, \tag{1}$$

TABLE I. Distance (measured on the line between anode and cathode) taken from the electrocoloration images along with the voltage drop corresponding to the region (anode) versus time.

Time (s)	Dark front distance (mm)	Voltage drop across anode (V)
240	1.81	178.5
360	1.78	192.8
420	1.64	193.8
520	1.63	194.9
630	1.63	195.6
800	1.63	196.3
960	1.60	196.8

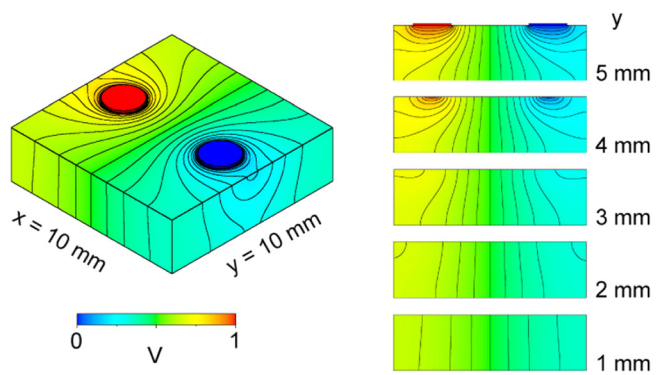

FIG. 4. 3D view of the electric field potential in the case of two round electrodes on top of the rectangular sample.

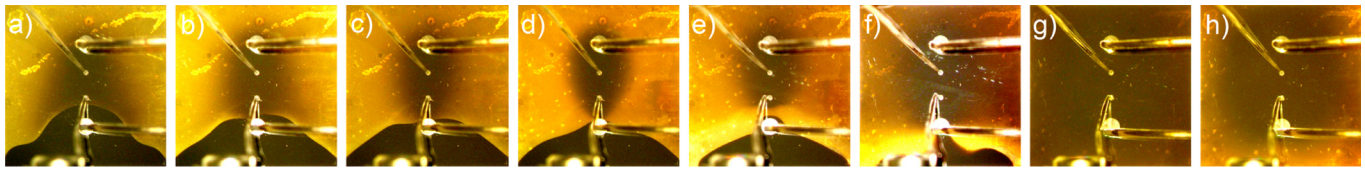

FIG. 5. Optical microscope images of electrocoloration process versus time: (a) 1.5, (b) 3.0, (c) 4.5, (d) 20, (e) 50, (f) 60, (g) 80, and (h) 100 h. Experimental conditions: temperature ~250 °C, pressure 10^{-8} mbar, voltage 200 V, current compliance 100 mA. The bottom electrode is the anode, while the top is the cathode.

where h is the average bubble height and P_0 is the pressure of oxygen inside the bubble. The assumed geometry in the model is presented in Fig. 7. D is flexural rigidity given by

$$D = \frac{Es^3}{12(1-v^2)}, \tag{2}$$

where s is the plate thickness, E is the Youngs modulus of the plate material, and v is the Poisson ratio of the plate material.

Taking the data from Ref. 25 for the mechanical properties of thin platinum films and data from AFM measurements, we were able to calculate the average oxygen pressure inside the bubble to be equal to 6.91×10^7 Pa. Combining this information with the average volume of the bubble and the temperature during the experiment, we were able to calculate the approximate number of oxygen ions trapped in the bubble. We adopted the equation of state given by the Redlich-Kwong equation of state modified by the Soave equation of state[26] with the critical parameters for the oxygen taken from the literature[27] and obtained the value of $n = 2.0 \times 10^8$ per bubble. Using optical microscopy, we found approximately 10^5 bubbles in the anode area, thus, allowing us to estimate the total amount of oxygen released under the anode electrode during electrocoloration to be close to 2×10^{13} or 10^{14} cm^{-3} in terms of volume. It must be kept in mind that this value is the lower limit for the amount of released oxygen due to the partial transparency of the platinum films[28] or the fact that not all released oxygen could be trapped under the electrode. Although this value cannot be compared directly with other types of measurements, we can try to place it in the context of the oxygen release under the high vacuum condition and elevated temperature in effusion experiments. In the case of undoped STO, the value of 3×10^{14} cm^{-3} was reported[7] to be very close to our result. On the other hand, we cannot be sure that this amount of oxygen was in fact completely removed from the crystal; it could be possible that after the electroformation experiment, that part of oxygen trapped inside the bubbles (high pressure of $P = 6.91 \times 10^7$ Pa) was incorporated back into the crystal. Moreover, a nice example of filamentary transfer can be found in the sample after electrocoloration, namely, the formation of stripes following the [100] and [010] directions emerging from the anode and propagating towards the cathode—in Fig. 6(b). The temperature measurement was performed after some hours of electrocoloration. At the 20th hour of the experiment, all parts of the sample displayed semiconducting behavior—Fig. 8(a). The total resistivity at room temperature decreased to 4 kΩ. After the next 60 h, the resistivity dropped further to 100 Ω as seen in Fig. 8(b). Moreover, the electrical behavior of the electrodes and the interior of the sample changed from semiconducting to metallic behavior. We continued the experiment for a total time of 100 h resulting in the resistivity decreasing to 50 Ω at room temperature. It can be observed that the changes in electrical behavior can be correlated with color changes as seen in Figs. 5(d), 5(g), and 5(h). A slightly new color with blurred edges emerged from between the electrodes, slowly expanding to the whole

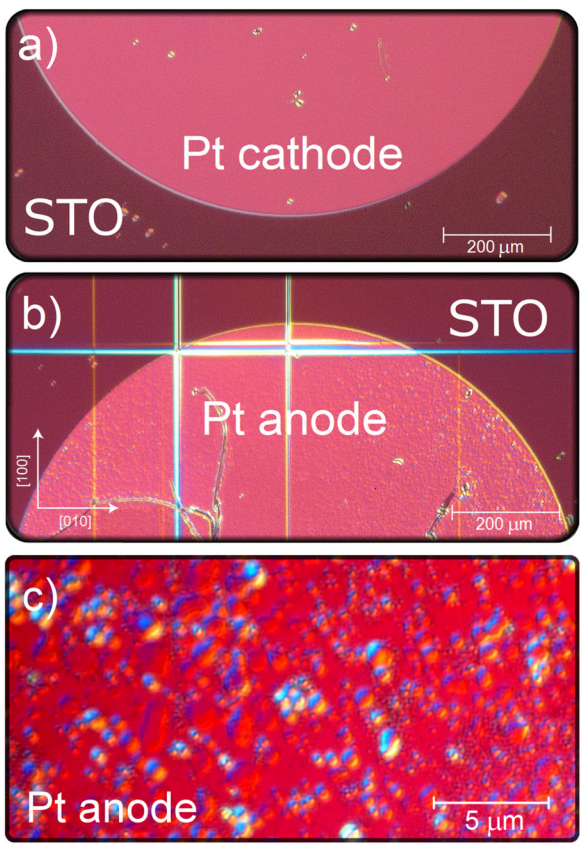

FIG. 6. Images from the optical microscope (phase contrast) showing the sample after electrocoloration: (a) in the cathode region, (b) in the anode region, (c) magnification of the anode region.

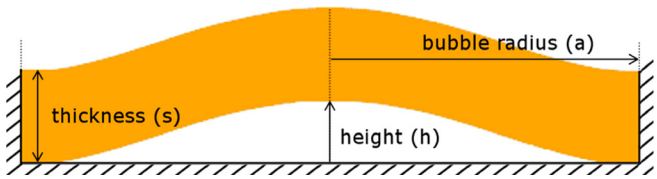

FIG. 7. Bubble geometry along with the description for the oxygen pressure calculations.

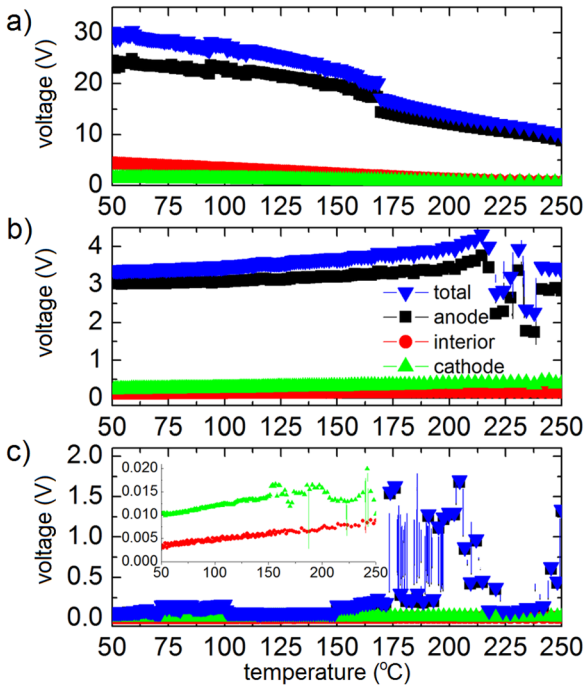

FIG. 8. Electrical behavior of the sample as a function of temperature at different times of the electrocoloration experiment after: (a) 20, (b) 80, and (c) 100 h of electrocoloration.

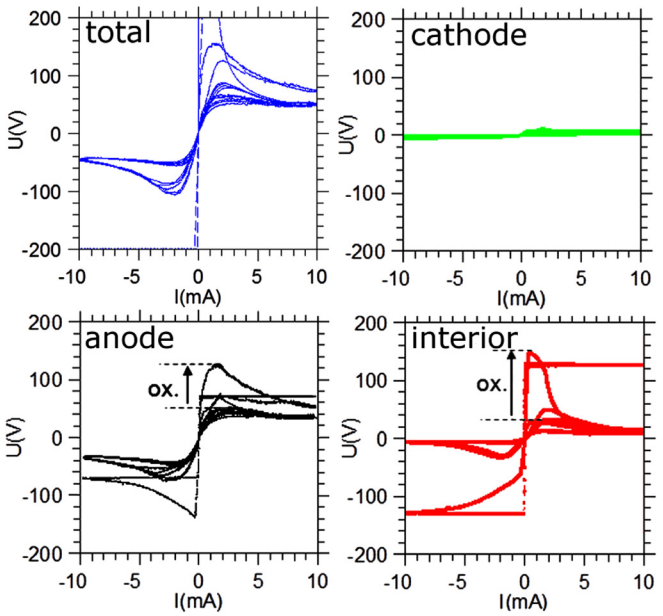

FIG. 9. The voltage-current characteristics after electroreduction. The total resistivity was measured between the anode and cathode, while the bulk contribution was measured between the inner electrodes.

sample. The dark region of oxidized STO as well as the bright yellow color of the reduced STO shrank leaving a uniformly colored sample after 80 h—Fig. 5(g). Judging from the electrical measurements and from the fact that the new color emerged from the region between the anode and cathode where the oxygen vacancy concentration is highest[19] we can conclude that it originates from the high electron concentration (compensating high $[V_O^{\cdot\cdot}]$ concentration). This is consistent with the fact that thermally reduced samples are also much darker than before reduction and that during our experiment the oxygen was continuously removed both by electric field and thermal reduction (substantial Joule heating at reducing atmosphere of 10^{-8} mbar). After approximately 100 h, we concluded the experiment and optical images of the sample were made—Fig. 5(h). The edges of the crystal became brighter, again beginning from the region with the highest defect concentration (edge). Looking closely at the temperature measurements, indications of resistive switching phenomena can be found—Fig. 8(b) and more clearly in (c). The rapid jumps in the resistivity, observed only near the anode, are related to switching between the on and off states by the conducting filaments. When the measurement was made, the system was far from equilibrium, therefore, the removal of oxygen due to the electric field was countered by the migration of oxygen from the bulk through the network of extended defects, causing observable random changes in the conductivity. To confirm the RS behavior, the voltage-current (V-I) characteristics were recorded at different partial pressures—Fig. 9. The RS hysteresis is clearly visible, and is limited to the bulk and the anode, while there is no hysteresis at the cathode. We conclude that a very high concentration of oxygen vacancies at the cathode prevents the switching, and thus, the cathode is always in the on (low resistance) state. It could be predicted that by increasing the oxygen partial pressure at the surrounding atmosphere, the RS behavior would increase thanks to the additional oxygen incorporated into the sample. The effect of increasing the pressure to 10^{-1} mbar is indexed by the ox arrow in Fig. 9. Indeed, the RS hysteresis is extended, proving that the system is very

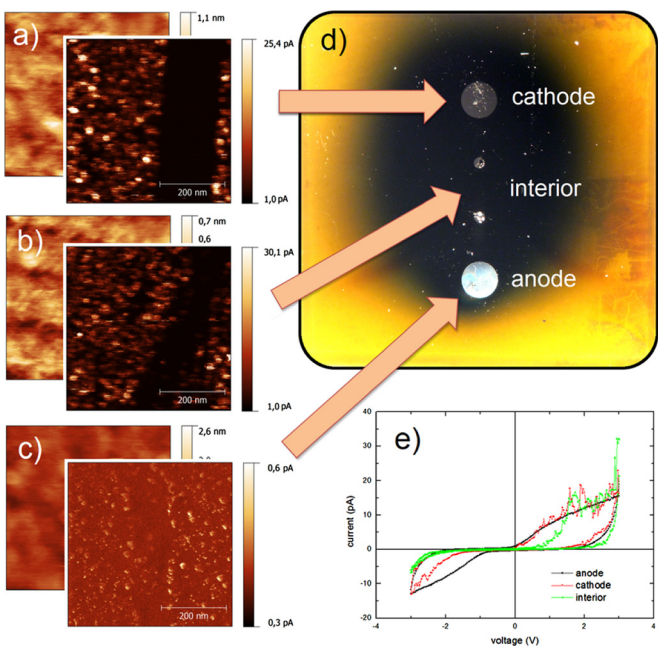

FIG. 10. LC-AFM measurements of the sample after electroreduction. The topography and local conductivity maps for: (a) cathode, (b) interior, and (c) anode are presented. Optical image of the sample after electroreduction and re-oxidation in ambient atmosphere (d). The RS behavior of different components measured by the conducting tip (e).

susceptible to the oxygen pressure in the ambient environment. The observed changes were almost instantaneous, indicating that the process of incorporating the atmospheric oxygen into the lattice (bulk) is very fast (thanks to the presence of fast diffusion paths). Finally, after the experiment, samples were removed and transported *ex situ* into the UHV AFM/STM system. During this process, due to re-oxidation at ambient atmosphere, the color further changed into the situation visible in Fig. 10(d). The brownish/yellow color observed in the virgin sample was partially restored at the sample edges. The local conductivity AFM experiments performed in different regions are consistent with the previous results. The voltage applied to the conducting tip was set to -3 V for all measurements. The topography and the local conductivity maps are presented in Figs. 10(a)–10(c). The cathode and the interior regions are display good conductivity, showing a large number of conducting spots (with a diameter of $10-12$ nm)—the exits of the extended defects. At the same time, the anode region is poorly conducting. The RS behavior is also confirmed, as visible in Fig. 10(e) showing that also in the nanoscale, the anode exhibits the greatest changes in conductivity.

IV. CONCLUSIONS

We have shown that by means of the electrical stimuli we were able to induce the metal-insulator transition in a single crystal of strontium titanate doped with iron. Moreover, the dynamics of the MI transition, combined with the formation of streaks between the electrodes during the electroformation on the macro-scale and inhomogeneous conductivity on the surface on the nano-scale, indicate the existence of fast ion transport paths (filaments) and the network of extended defects. The question concerning the exact nature of the enhanced ion transport remains open, in particular, if the ion (oxygen vacancy) mobility is increased due to the lower symmetry in extended defects compared to the volume or if the fast transport may be caused by a local thermal excitation (regarding a filament as a "heating rod" due to the higher electronic conductivity along extended defects). The electrocoloration experiment demonstrated a strong connection between the evolution of the color front and the electrical properties of the investigated crystal. The resistive switching was also clearly shown, both on the large and small scale. Additionally, calculations of the total amount of oxygen removed from the crystal were performed, based on the formation of oxygen bubbles under the platinum electrode.

ACKNOWLEDGMENTS

We gratefully acknowledge the support of the SFB 917 funded by the Deutsche Forschungsgemeinschaft. Additionally, one of the authors (M.W.) is grateful for financial support from the DoktroRIS program funded by the European Union through the European Social Funds (ESF).

[1]R. A. de Souza, J. Fleig, R. Merkle, and J. Mier, Z. Metallkd. **94**, 218 (2003).
[2]D. M. Hill, H. M. Meyer III, and J. H. Weaver, J. Appl. Phys. **65**, 4943 (1989).
[3]R. Astala and P. D. Bristowe, J. Phys: Condens. Matter **14**, 13635 (2002).
[4]K. Szot, W. Speier, G. Bihlmayer, and R. Waser, Nature Mater. **5**, 312 (2006).
[5]R. Waser, R. Dittmann, G. Staikov, and K. Szot, Adv. Mater. **21**(25–26), 2632–2663 (2009).
[6]K. Szot, W. Speier, and W. Eberhardt, Appl. Phys. Lett. **60**(10), 1190–1192 (1992).
[7]K. Szot, W. Speier, R. Carius, U. Zastrow, and W. Beyer, Phys. Rev. Lett. **88**, 075508 (2002).
[8]K. Szot, M. Rogala, W. Speier, Z. Klusek, A. Besmehn, and R. Waser, Nanotechnology **22**(25), 254001 (2011).
[9]G. A. Cox and R. H. Tredgold, Br. J. Appl. Phys. **16**, 427–430 (1965).
[10]J. Blanc and D. L. Staebler, Phys. Rev. B **4**, 3548 (1971).
[11]R. Waser, T. Baiatu, and K. H. Hardtl, J. Am. Ceram. Soc. **73**, 1654–1662 (1990).
[12]T. Baiatu, R. Waser, and K. H. Hardtl, J. Am. Ceram. Soc. **73**, 1663–1673 (1990).
[13]I. Denk, F. Noll, and J. Maier, J. Am. Ceram. Soc. **80**(2), 279–285 (1997).
[14]J. Seidel, W. Luo, S. J. Suresha, P.-K. Nguyen, A. S. Lee, S.-Y. Kim, C.-H. Yang, S. J. Pennycook, S. T. Pantelides, J. F. Scott, and R. Ramesh, Nat. Commun. **3**, 799 (2012).
[15]S. Steinsvik, Ph.D. dissertation, Olso, 1999.
[16]J. F. Scott, S. A. T. Redfern, M. Zhang, and M. Dawber, J. Eur. Ceram. Soc. **21**(10–11), 1629–1632 (2001).
[17]R. Wang, Y. Zhu, and S. M. Shapiro, Phys. Rev. Lett. **80**, 2370 (1998).
[18]D. M. Smyth, Annu. Rev. Mater. Sci. **15**, 329–357 (1985).
[19]M. Janousch, G. I. Meijer, U. Staub, B. Delley, S. F. Karg, and B. P. Andreasson, Adv. Mater. **19**, 2232 (2007).
[20]Z. J. Kiss, Phys. Today **23**(1), 42 (1970).
[21]B. W. Faughnan, Phys. Rev. B **4**(10), 3623–3636 (1971).
[22]C. Lenser, A. Kalinko, A. Kuzmin, D. Berzins, J. Purans, K. Szot, R. Waser, and R. Dittmann, Phys. Chem. Chem. Phys. **13**, 20779–20786 (2011).
[23]J. J. Yang, F. Miao, M. D. Pickett, D. A. Ohlberg, D. R. Stewart, C. N. Lau, and R. S. Williams, Nanotechnology **20**, 215201 (2009).
[24]S. Timoshenko and S. Woinowsky-Kreiger, *Theory of Plates and Shells*, 2nd ed. (McGraw-Hill Higher Education, New York, 1964).
[25]A. L. Romasco, L. H. Friedman, L. Fang, R. A. Meirom, T. E. Clark, R. G. Polcawich, J. S. Pulskamp, M. Dubey, and C. L. Muhlstein, Thin Solid Films **518**(14), 3866–3874 (2010).
[26]G. Soave, Chem. Eng. Sci. **27**, 1197–1203 (1972).
[27]G. Liessmann, W. Schmidt, and S. Reiffarth, "Data compilation of the Saechsische Olefinwerke Boehlen," Germany, 1995, p. 12.
[28]R. Schmiedl, V. Demuth, P. Lahnor, H. Godehardt, Y. Bodschwinna, C. Harder, L. Hammer, H.-P. Strunk, M. Schulz, and K. Heinz, Appl. Phys. A **62**(3), 223–230 (1996).